AIAA JOURNAL
Vol. 47, No. 10, October 2009

Comparison of Hot-Fire and Cold-Flow Observations of Nitrogen Tetroxide/Monomethylhydrazine Impinging Combustion

Tony Yuan,* Cetera Chen,† and Berlin Huang‡
National Cheng-Kung University, Tainan 701, Taiwan, Republic of China

DOI: 10.2514/1.41003

The combustion phenomena of doublet impingements of nitrogen tetroxide and monomethylhydrazine were observed in this research. The total flow rates of the propellants were controlled at ∼8.00 g/s to simulate the operation of a 5 lbf rocket, and the ratios of the mass flow rates (O/F) of nitrogen tetroxide and monomethylhydrazine were varied from 1.0 to 2.5. With a two-axis translation module, a C-type thermocouple was used to measure the two-dimensional temperature distributions of the flames at 20 mm downstream of their impinging points. The observations showed that induction distances always appeared from the positions of propellants' impingement to ignition, and the ignition was induced by the local concentrations of gaseous monomethylhydrazine. The maximum flame length of ∼80 mm appeared at the best mixing condition of $O/F = 1.2$, and diffusion-type flames at higher O/F showed shorter flame lengths for poor mixing after the flames had been ignited. Comparing to the previous cold-flow observations by the planar laser induced fluorescence technique with simulants of water- and chloroform-based solutions to match the densities, viscosities, and surface tensions of monomethylhydrazine and nitrogen tetroxide, the locations of high-temperature zones in hot-fire experiments were adequately described by the calculated two-dimensional temperature distributions from the observed local mixture ratio data at the corresponding ignition positions in the cold-flow experiments. These results inferred that the mixture ratio profile was almost conserved after ignition. That is, by properly analyzing the mass distribution of the cold-flow observation with simulants, the temperature distribution of the impinging combustion of nitrogen tetroxide/monomethylhydrazine can be predicted.

Nomenclature

d	=	orifice diameter of injector
E_m	=	mixing efficiency
$\dot{m}$	=	mass flow rate
Nu	=	Nusselt number
O/F	=	mass flow rate ratio of oxidizer (nitrogen tetroxide) and fuel (monomethylhydrazine)
T_g	=	corrected flame temperature
T_j	=	measured flame temperature
T_{peak}	=	peak flame temperature
$T_{x,y}$	=	local adiabatic flame temperatures
T_∞	=	room temperature
v	=	jet velocity
ε	=	emissivity of the materials of thermocouple
λ	=	thermal conductivity of the gas
ψ	=	Stefan–Boltzmann constant of thermal radiation

I. Introduction

THE applications of low-thrust nitrogen tetroxide/monomethylhydrazine (NTO/MMH) bipropellant thrusters are mainly on the reaction control of missiles and satellites for its storable, hypergolic, and superior specific-impulse characteristics. Although NTO/MMH possesses hypergolic characteristics, their impinging combustion still follows the conventional spray combustion pattern. Droplets were observed experimentally in the NTO/MMH burning spray [1], and the autoignition as well as the following combustion process proceeds mainly in the gas phase [2]. The impingement provides the energy and momentum required for atomization and mixing that take place in the immediate vicinity of the impinging point.

It is obvious that the mixing of the propellants is crucial for the combustion control of NTO/MMH thrusters. Factors such as momentum flux of the impinging jets, physical properties of fluids, and the design of the injector may alter the mass distribution of liquids significantly. Rupe [3,4] investigated the mixing of doublet impinging jets and defined the mixing condition from the calculation of the mixing efficiency. He proposed that the momentum and the diameter of the impinging jets must be equal to acquire the optimum uniformity and the best mixing efficiency. The same conclusions were made in the observations of doublet and split-triplet impingements made by Won et al. [5]. Riebling [6] extensively reviewed the mixing data in the literature and deduced a correlation of area ratio, density ratio, and mixture ratio to the optimum mixing efficiency. In his correlation, the mixture ratio was the most significant factor to the mixing efficiency. The mixing mechanism proposed by Ashgriz et al. [7] concluded that the momentum of the impinging jets affected the mixing of the liquids before atomizing, and, when the liquid jets disintegrated into droplets, the turbulent dispersion would improve the mixing of the liquids.

Instead of using the conventional mechanical patternator, the mass distributions of sprays were analyzed by Koh et al. [8] and Jung et al. [9] with the planar laser induced fluorescence (PLIF) technique. Their optical measurements were justified by comparing the optical data to that from a mechanical patternator. Besides the high-resolution and nonintrusive characteristics of the PLIF technique, by taking the ratios of the fluorescent signals and the scattering signals of droplets, the Sauter mean diameter (SMD) distribution of droplets may also be deduced with careful calibration [10]. A similar technique was used to observe the mass distribution in unlike-doublet impinging sprays by Yuan and Chen [11]. They demonstrated that both the momentum flux of the jets and the surface tension of the fluids significantly affected jet atomization

Received 15 September 2008; revision received 25 February 2009; accepted for publication 16 April 2009.

*Associate Professor, Institute of Aeronautics and Astronautics, Department of Aeronautics and Astronautics, No. 1, Dasyue Road; yahn@mail.ncku.edu.tw.

†Postdoctoral Student, Institute of Aeronautics and Astronautics, Department of Aeronautics and Astronautics.

‡Graduate Student, Institute of Aeronautics and Astronautics, Department of Aeronautics and Astronautics.

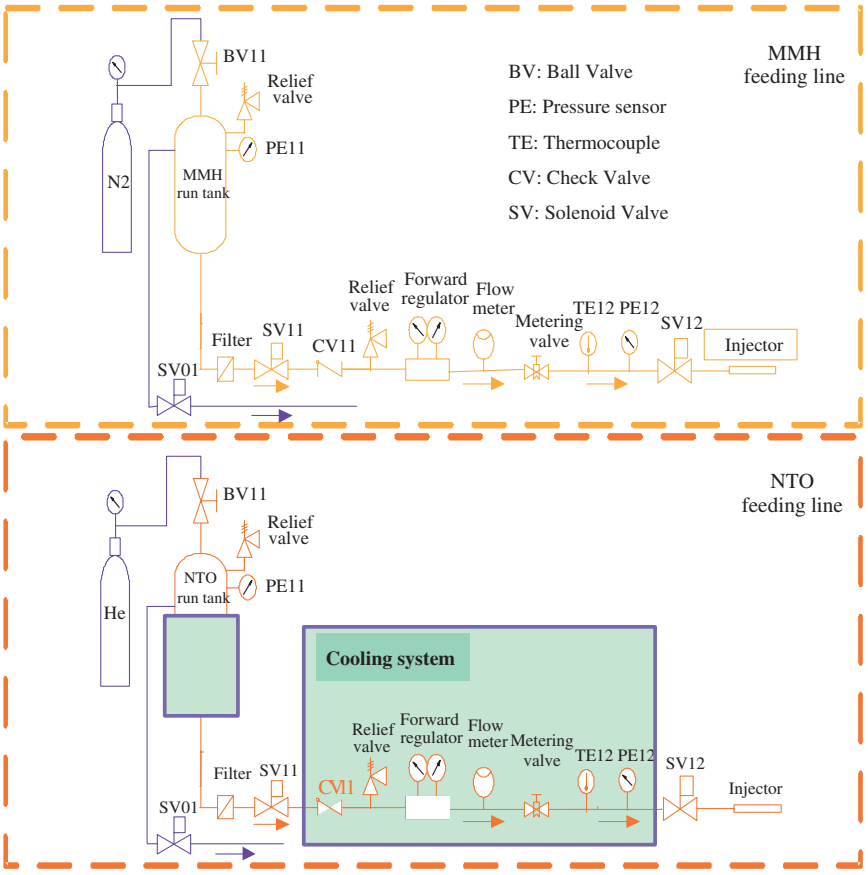

Fig. 1 Schematic illustration of the flow control system.

and spray uniformity. The cold-flow observations of NTO/MMH impinging sprays with simulants of water- and chloroform-based solutions were also performed by Yuan et al. [12]. The distributions of mixture ratios and pseudoflame temperatures were deduced from the local mass distribution data in their study. They concluded that the optimum characteristic exhaust velocity existed at overall mass ratios of NTO to MMH in the range of 1.2–1.4 with 0.3/0.3 mm orifices and a $+30/-30$ deg impinging angle.

Although the cold-flow studies provided an assessment of the hot-fire phenomena of NTO/MMH, the factors, such as the hypergolic characteristics, thermal expansion of the hot gas, and the prevaporization of NTO and MMH may cause the hot-fire phenomena to differ from that predicted from the cold-flow observations. To verify the adequacy of the cold-flow predictions, this research investigated the open-flame phenomena of doublet impinging combustion of NTO/MMH by imaging technique and thermocouple measurements. The combustion phenomena of these hot-fire experiments were analyzed and compared with that from the cold-flow predictions.

II. Experimental Method

Nitrogen-compressing (for MMH) and helium-compressing (for NTO) fluid supply systems were used to control the propellant flow rates in this study (Fig. 1). Two turbine-type flow meters (Sponsler, model MF20) with an accuracy of 0.25% of the reading were used to monitor the mass flow rates of the propellants. In the cold-flow observations, water- and chloroform-based solutions were used as simulants to match the density, viscosity, and surface tension of MMH and NTO, respectively [12]. The two simulants are immiscible and the physical properties of the simulants are listed in Table 1. The flow control system was carefully calibrated and the components as well as the tubing of the system were all made of sus316 with a Teflon seal to be compatible with the chemical properties of NTO and MMH.

The injector's orifices were oriented to have a $+30/-30$ deg impinging angle. The diameters (0.304 and 0.307 mm, inner diameter), the roundness, and the smoothness of the orifices were carefully verified by visual inspection of the images of water jets (Fig. 2). By controlling the total flow rate of $\sim$8 g/s to meet the operation specification of a 5 lbf NTO/MMH rocket, these single-pair doublet impinging combustion experiments were performed. To compare these hot-fire results with the previous cold-flow studies [12], the mass flow rate ratios (O/F) of NTO and MMH were varied from 1.0 to 2.5. In the engineering design, theO/F was usually controlled at $\sim$1.65, which is in the fuel-rich conditions (stochiomatric $O/F \approx 2.5$) [13,14].

Table 1 Physical properties of test fluids

Test fluid	Water, vol.%	Chloroform, vol.%	Methanol, vol.%	Density, ρ, g/cm^3	Viscosity, μ, 10^{-3} N·s/m^2	Surface tension, σ, 10^{-3} N/m	Saturated pressure, $P^{\text{sat}}_{300\text{ K}}$, kPa
MMH simulant	95	——	5	0.99	1.11	32.9 [a]	——
NTO simulant	——	95	5	1.41	0.57	25.7	——
		MMH		0.88	0.85	33.5	7.0
		NTO		1.45	0.42	26.5	166.2
		Water		1.00	0.89	71.8	3.8

[a]Surfactant added to decrease surface tension.

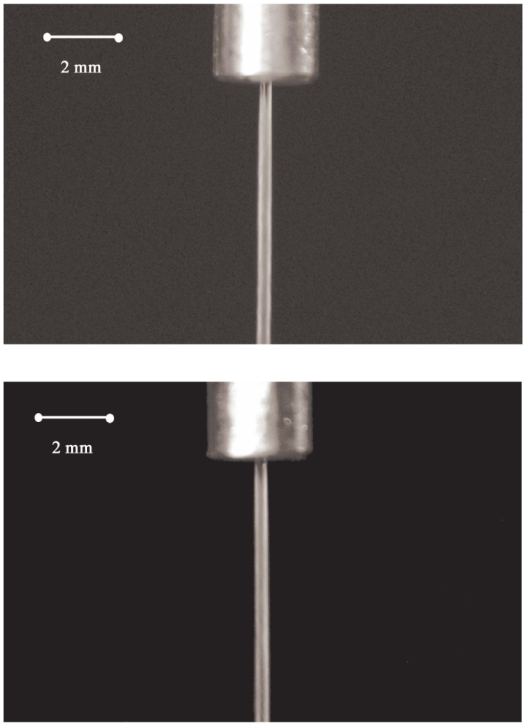

Fig. 2 Views (0 and 90 deg) of water ejection for orifice calibration ($V_j = 18$ m/s).

The flame images and the flame temperatures were acquired by charge-coupled device (CCD) cameras and a thermocouple array (Fig. 3), respectively. Two high-resolution pseudocolor CCD cameras (260×1960 pixels, shutter speed of 1000 μs) and a snapshot CCD camera (1504×1000 pixels, shutter speed of 750 μs) were used to observe the front- and side-view flame images.

From the calculation of the adiabatic flame temperature of NTO/MMH combustion, the reaction temperature can be as high as 3000 K [12]. In this study, a C-type thermocouple was used to measure the flame temperatures in the reaction zone (Fig. 3). Seven thermocouples were arranged in an array and the distance between each thermocouple was 10 mm. With a two-axis translation module, the thermocouple array measured the two-dimensional temperature distributions ($T_{x,y}$) in the hot-fire experiments with a spatial resolution of 5/0.1 mm at 20 mm downstream of the impinging point. The measured two-dimensional temperature ($T_{x,y}$) was carefully corrected from radiation heat loss by [15]

$$\Delta T = T_g - T_j = \frac{\varepsilon \psi d (T_j^4 - T_\infty^4)}{2\lambda \cdot Nu} \tag{1}$$

where ψ is the Stefan–Boltzmann constant of thermal radiation, T_∞ is the room temperature, and T_g, T_j are the corrected and measured flame temperatures, respectively. A value of 0.42 was used for the emissivity (ε) based on the materials of the thermocouple [16]. The thermal conductivity (λ) was evaluated for the gas of the equilibrium composition of $O/F = 2.4$, and the Nusselt number (Nu) was approximated based on the welded junction diameter ($d \approx 0.7$ mm). An estimated collective error of temperature measurements was ± 80 K.

III. Results and Discussion

Figure 4 shows the front- and side-view flame images near the impinging point of NTO and MMH jets at various O/F. The images indicated that an induction zone was always present after propellants' impingement and before their ignition. The vapor of NTO (or NO_2), with the reddish-brown color gas, appeared in the induction zone and at the outer layer of the flames because NTO was easy to break up and evaporate for its low surface tension and high vapor pressure (see Table 2). Because the spontaneous heat releasing reactions occur mainly in the gas phase [2], it is believed that a relatively small amount of MMH was also spontaneous vaporized and reacted with gaseous NTO to provide heat for further liquid vaporization. As the gaseous MMH density got more sufficient in the downstream, a greater amount of heat release from higher gas-phase reaction rates finally induced the ignition of the bright flame.

To characterize the induction zone, Fig. 5 shows a typical two-dimensional profile of constant light intensity contours of the front-viewed flame image and the corresponding plots of light intensity and the intensity gradient along the flame axis. In the figure, the flame axis was approximated by connecting the impinging point and the x-direction peak intensities in the flame. The intensity gradient plots clearly show a positive peak and a negative peak near the beginning and end of the flame zone. The induction distance and the flame length were thus defined as the distance in the z direction from the

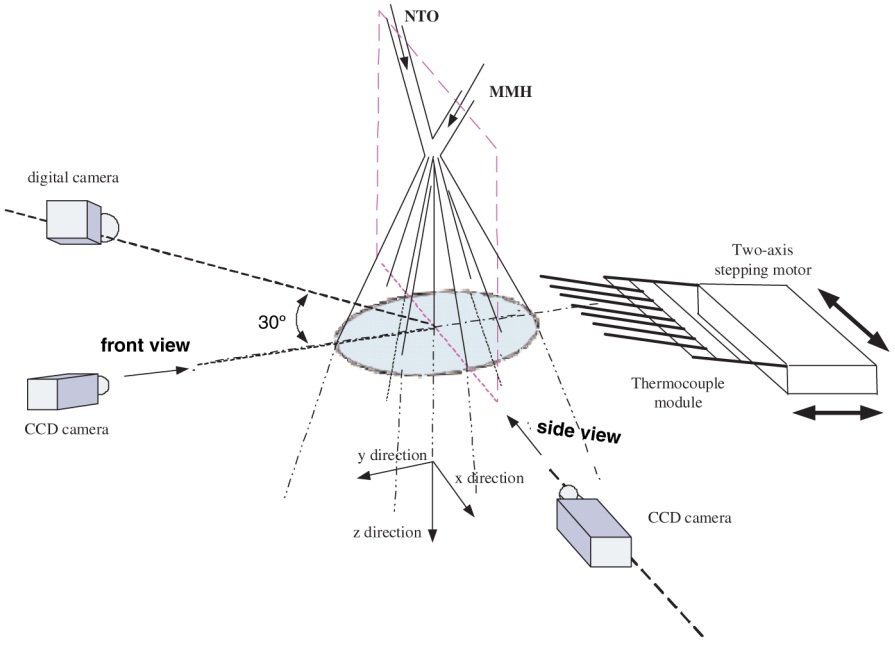

Fig. 3 Schematic of flame temperature and image acquisition systems.

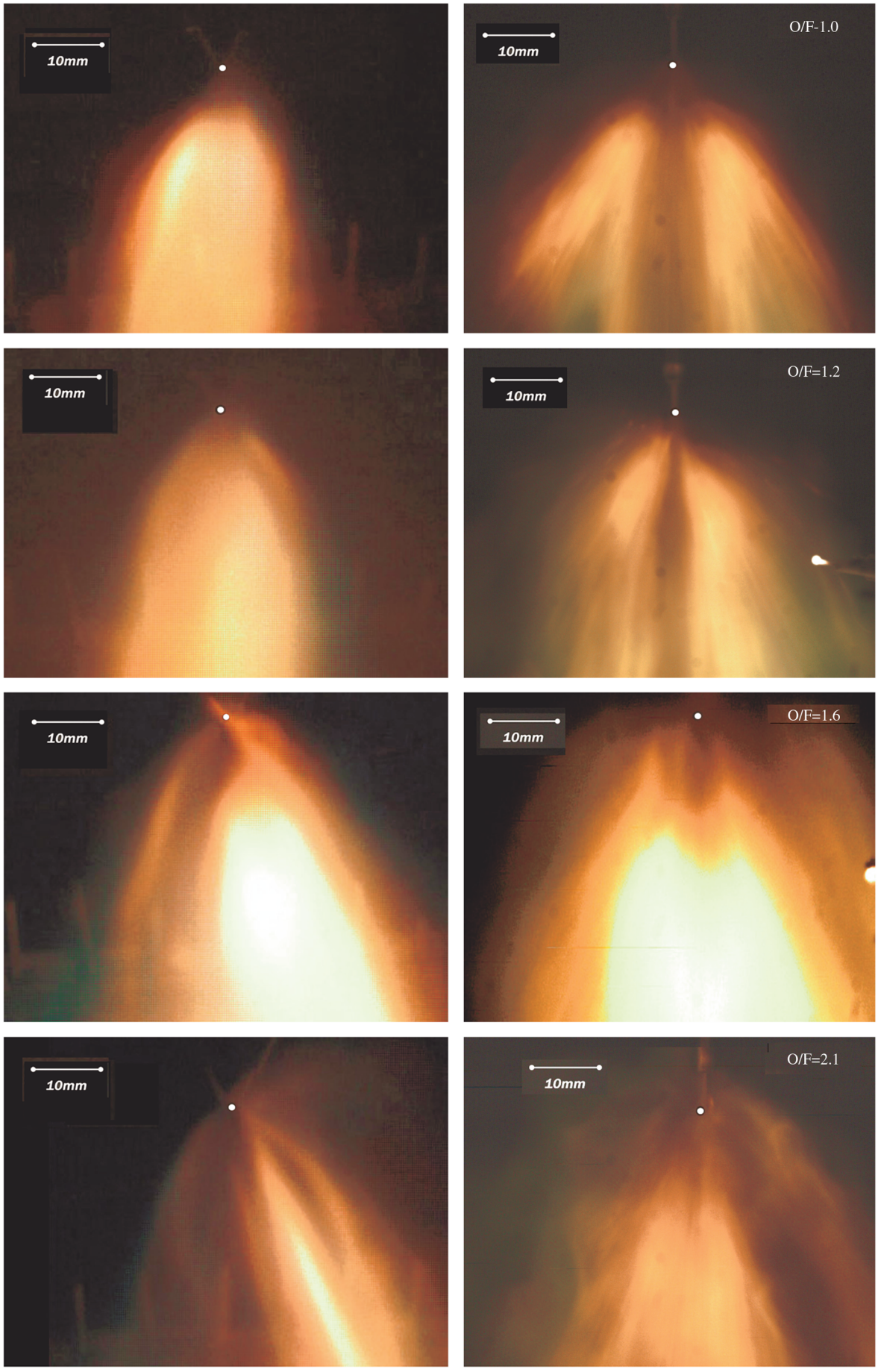

Fig. 4 Front-viewed (left) and side-viewed (right) flame images of NTO/MMH doublet impingements with constant total propellant flow rate of ∼8.0 g/s, where NTO was ejected from the left in the front-viewed images, and the white dot on each image was the impinging point.

Table 2 Experimental conditions and results of NTO/MMH doublet impinging combustion

O/F	NTO/MMH mass flow rate, g/s	NTO/MMH jet velocity, m/s	Momentum flux ratio $(\dot{m}_o v_o/\dot{m}_f v_f)$	T_{peak}, K	Induction distance, mm	Flame length, mm
1.0	3.95/3.95	38.5/63.5	0.61	2425	7.7	35.9
1.2	4.41/3.69	43.0/59.3	0.87	2790	10.0	79.2
1.4	4.65/3.22	45.4/51.8	1.27	2855	10.5	74.3
1.6	4.77/2.96	46.5/47.6	1.57	2676	10.3	70.4
1.8	5.18/2.94	50.5/47.3	1.88	2685	13.7	75.8
1.9	5.30/2.73	51.7/43.9	2.29	2754	12.4	65.3
2.1	5.45/2.59	53.1/41.6	2.68	2576	13.8	64.0
2.5	5.71/2.31	55.7/37.1	3.71	2425	8.0	73.6

impinging point to the position of the positive peak intensity gradient and the distance between the positions of two intensity gradient peaks, respectively. The induction distances and flame length at various O/F are plotted in Fig. 6.

Because the ignition of the propellants was controlled by the evaporation rate of MMH droplets, the impingement that produced smaller MMH droplets should have a shorter induction distance. At low O/F, high velocity MMH jets were impinged by relatively low velocity NTO jets and resulting in a sharp SMD distribution across the spray fan [17,18]. The fine MMH droplets produced mainly from aerodynamic instability distributed on the outer edge of the spray fan [19], hence the flames occurred from the outer edges as shown in the side-viewed images of Fig. 4, and have short induction distances as shown in Fig. 6. As the O/F increased, MMH jet velocities decreased and a smaller amount of fine MMH droplets was produced for their weakened aerodynamic instability. This resulted in longer induction distances, more uniform SMD distribution of MMH, and more uniform combustion as shown in the side-viewed images of Fig. 4. At $O/F \geq 1.8$, hydrodynamic instability dominated the disintegration and atomization of the MMH jets due to the impingement of a high velocity NTO jet. The effect of stronger hydrodynamic instability offset the effect of weaker aerodynamic instability on small MMH droplets production. Thus, the observation showed that the increase of induction distance almost ceased and even decreased at $O/F = 2.5$.

The local flame temperature of NTO/MMH impinging combustion depends mainly on the local mixture ratio and the rate of radiative heat loss. The planar high-temperature (>1800 K) distributions of NTO and MMH impinging combustion measured at 20 mm downstream of the impinging point are shown as the area enclosed by dark (blue) lines in Fig. 7, whereas the peak temperatures for various flames are listed in Table 2. The peak temperatures increased as the NTO supply increased because the experimental O/Fs were all in the fuel-rich conditions. However, at $O/F > 1.6$, the mixing efficiency started to decrease because the NTO jets were too strong to disintegrate and mix with MMH properly. The resulting incomplete combustion accounted for the decrease of the peak temperatures at higher O/F.

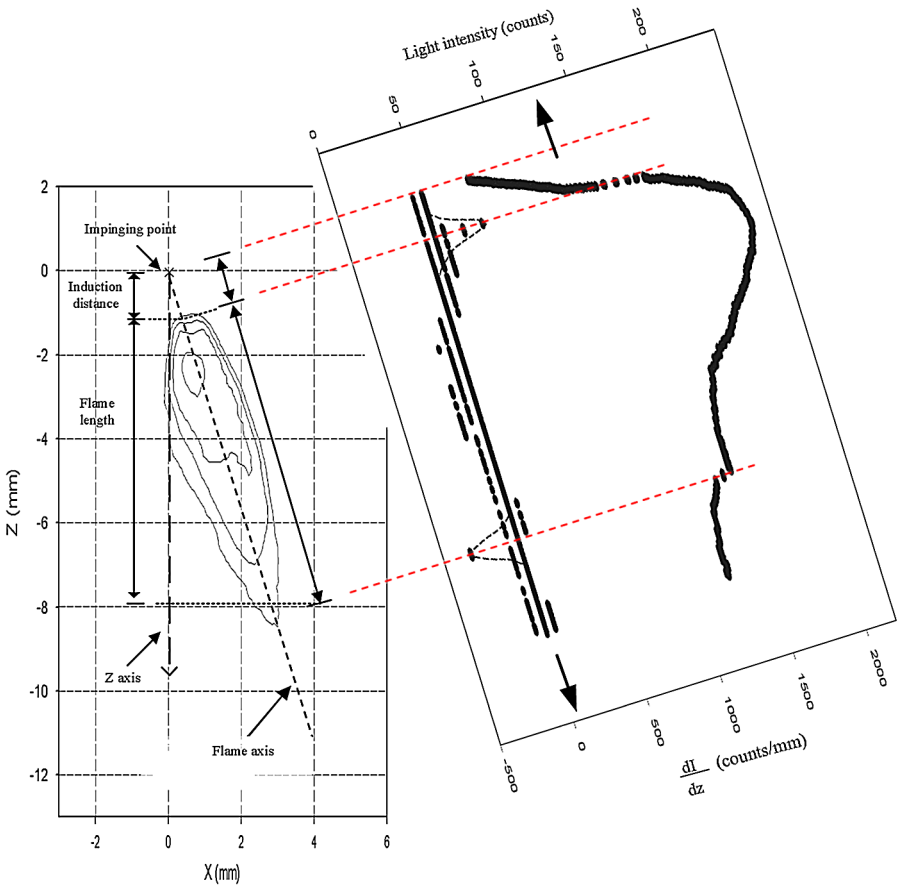

Fig. 5 Two-dimensional constant light intensity contours (left) and the corresponding light intensities and the intensity gradients along the flame axis (right) of the front-viewed flame image at $O/F = 1.6$.

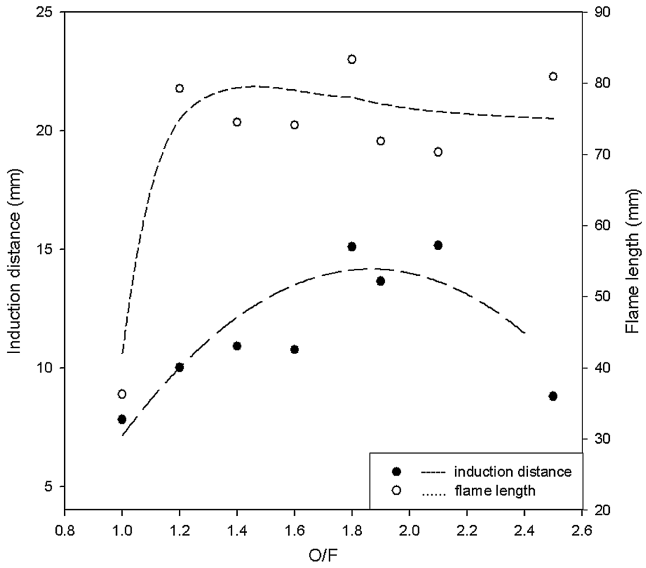

Fig. 6 Profiles of induction lengths and intensive reaction lengths at various O/F of NTO/MMH doublet impinging combustion.

By using the simulants of NTO and MMH, the mass probability distributions of the impinging spray at 10 mm downstream of the impinging point were observed by the PLIF technique and are shown in Fig. 8 [12]. The figure indicates that a relatively concentrated spray of MMH simulant mixed with and was surrounded by a relatively uniform distributed NTO simulant at $O/F = 1.0$. This mixing behavior explained the observation of a rather short flame length (~36 mm) in the corresponding hot-fire experiment due to quick consumption of NTO at this highly overall fuel-rich condition; and because some of the heat release was used to evaporate the concentrated MMH droplets, a low peak flame temperature was also observed (see Table 2). A better mixing occurred at $O/F = 1.2$; the increasing amount of NTO resulted in a longer flame length (~80 mm) as well as higher peak flame temperatures. For $O/F > 1.2$, a stronger NTO jet induced lean combustion in the NTO droplets concentrated core region. The combustion became a partially premixed diffusion flame with oxidizer in the core. Not having an effective mixing mechanism in the downstream to transport MMH to the NTO concentrated core in these open-flame experiments, the flames were distinguished when the core NTO consumed the adjacent MMH, and the flame lengths decreased slightly as O/F increased from 1.2.

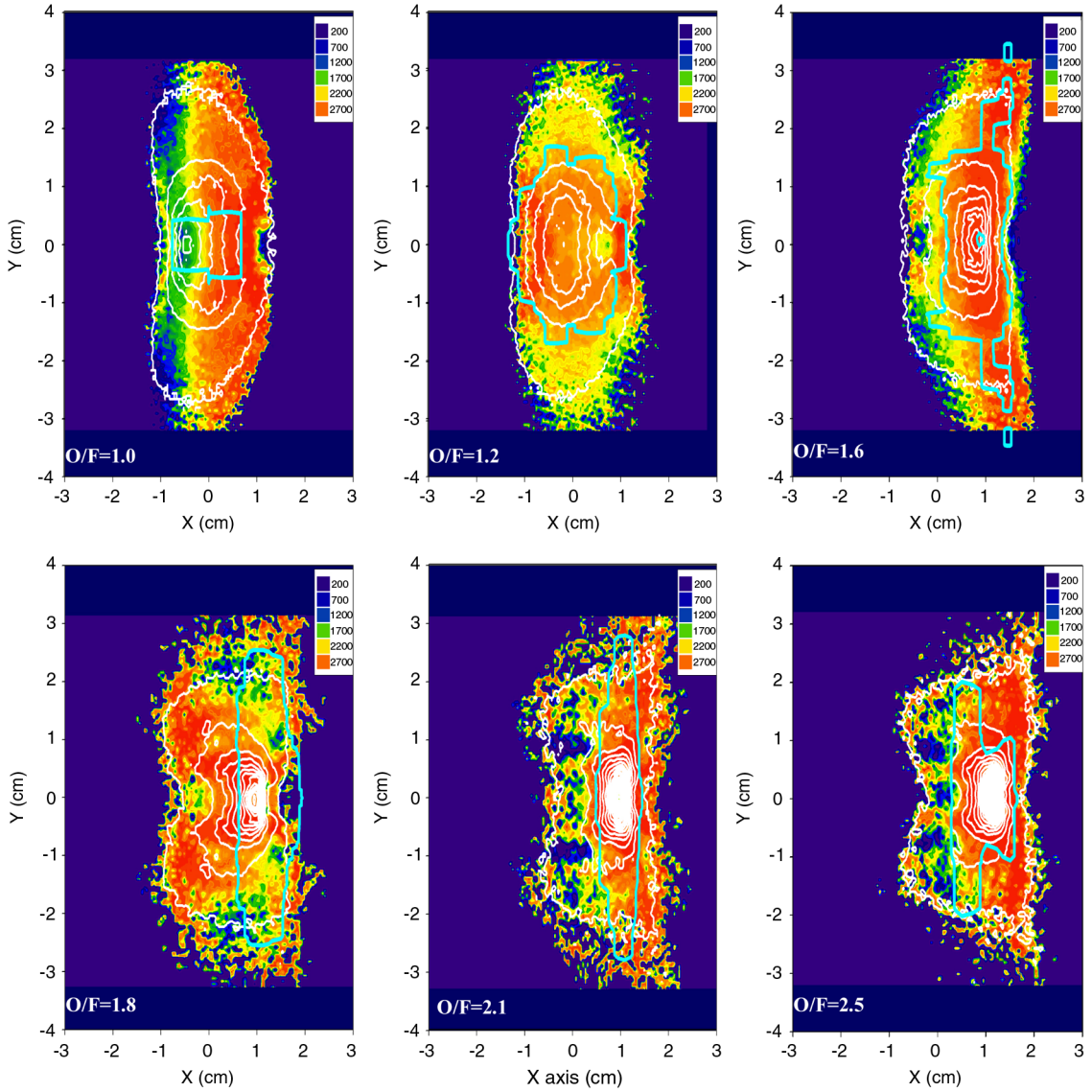

Fig. 7 Calculated temperature distributions and the constant probability density distributions of mass (white lines) based on the cold-flow measurements of NTO/MMH simulants at 10 mm downstream of the impinging point [12]. The outer probability density contour of mass was 5×10^{-4} mm^{-2} and the increment between contours was 3×10^{-3} mm^{-2}. The dark (blue) line enclosed the area of measured flame temperatures in impinging combustion of NTO/MMH above 1800 K (this work).

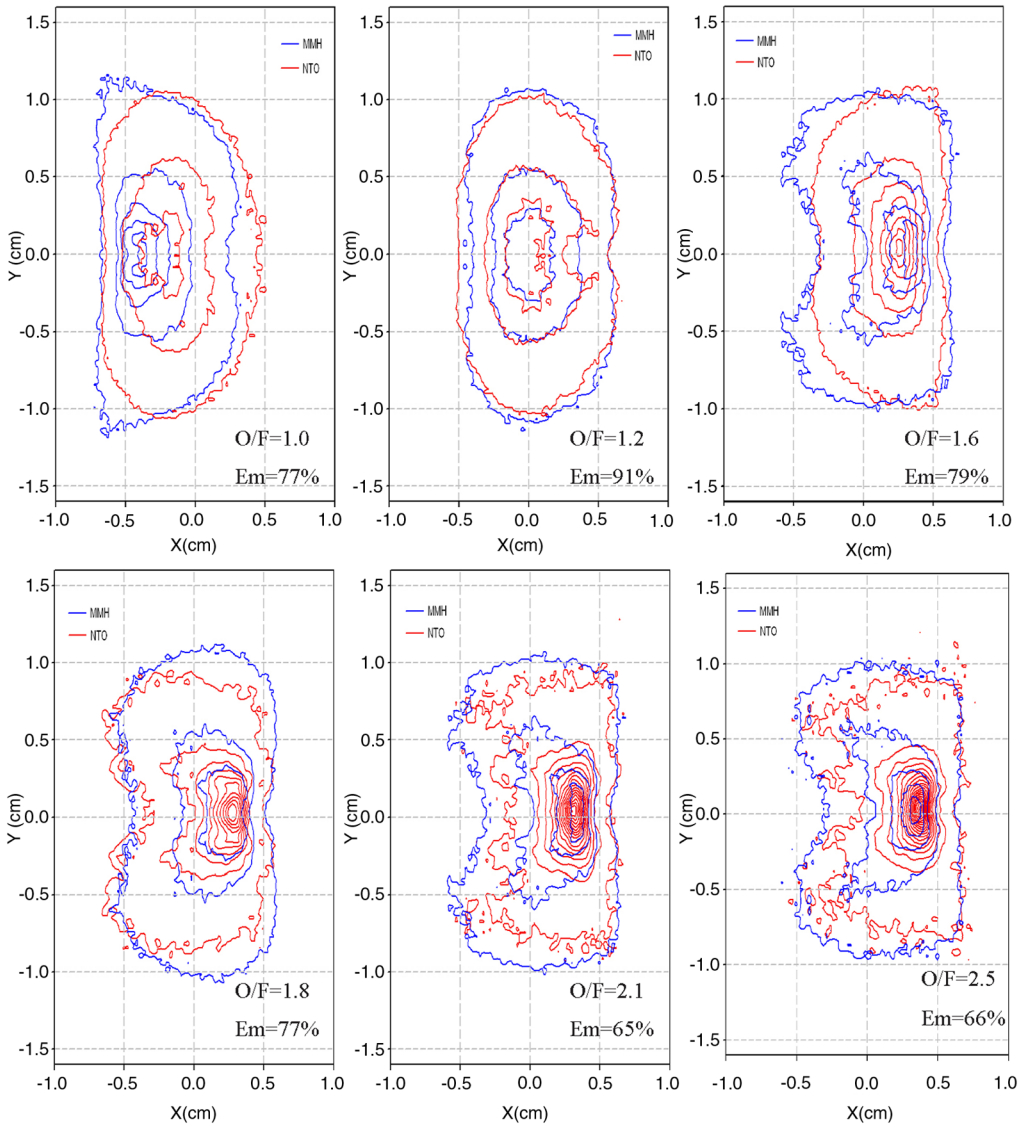

Fig. 8 Two-dimensional mass probability density distributions of MMH simulant (dark, blue) and NTO simulant (gray, red) at 10 mm downstream of the impinging point for doublet impingements. The outer contour of the constant probability density was 5×10^{-4} mm^{-2} and the increment between contours was 3×10^{-3} mm^{-2} [12].

Besides the mass probability, distributions of simulants were determined in the cold-flow experiments, and the distributions of local mixture ratios as well as the local adiabatic flame temperatures were also deduced [12]. By projecting the cold-flow data to 20 mm downstream to compare with that from the hot-fire temperature measurements, the observed mass probability distributions, the predicted high-temperature distributions, and the measured high-temperature distributions at various O/F are shown in Fig. 7. For flames of O/F from 1.2 to 1.6, where the induction distances ($\approx$10 mm) were near the cold-flow observation position ($=$10 mm), the positions and shapes of the measured high-temperature zones well matched with the predicted high-temperature zones from the cold-flow analyses. However, for flames of O/F from 1.8 to 2.1, where the ignitions (induction distances $=$ 12.4–13.8 mm) were downstream of the cold-flow observation position, the predicted high-temperature zones slightly shifted to the left of the measured high temperatures, while for O/F of 1.0 and 2.5, which had shorter induction distances (7.7 and 8.0 mm), the calculated high-temperature zones shifted to the right instead.

The observations of cold-flow experiments in Fig. 8 showed that MMH and NTO simulants individually had different spray patterns. Therefore, their mutual penetration and the secondary impingements of droplets of MMH and NTO simulants will cause the change of mixing behavior along the downstream of the spray fan [7]. The above relative positioning of the predicted and the measured high-temperature zones inferred that the temperature distribution and the mixture ratio distribution of the impinging spray were almost conserved after the propellants had been ignited. This scenario was verified by remeasuring the two-dimensional mass distribution of the simulants at the ignition location of each corresponding O/F flame. By using the local mixture ratios measured with simulants at the corresponding ignition positions observed in the hot-fire experiments (7.7, 10.0, 10.3, 13.7, 13.8, and 8.0 mm downstream of impinging point for O/F of 1.0, 1.2, 1.6, 1.8, 2.1, and 2.5, respectively) to calculate the adiabatic flame temperatures, the results which are shown in Fig. 9 indicated that the predicted flame temperature distributions based on the cold-flow measurements matched well with the high-temperature zone measured in impinging combustion of NTO/MMH at all O/F. A possible reason is that the ignition of the propellants at the end of the induction distance released a large amount of heat to vaporize most of the liquid droplets. The vaporization of liquid droplets prohibited further mutual penetration of propellants and conserved the mixing characteristics.

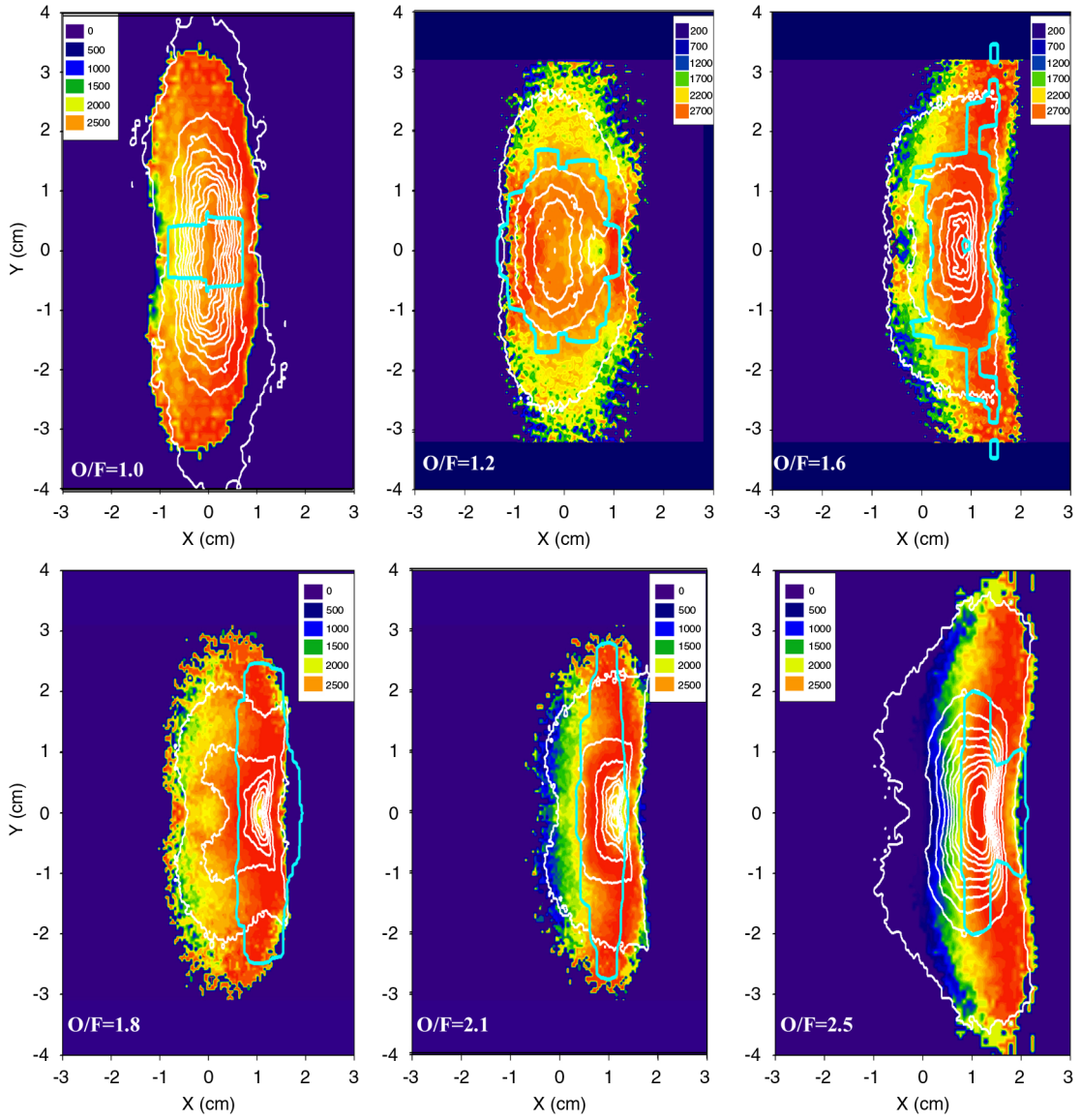

Fig. 9 Calculated temperature distributions and the constant probability density distributions of mass (white lines) based on the cold-flow measurements of impinging NTO/MMH simulants at 7.7, 10.0, 10.3, 13.7, 13.8, and 8.0 mm downstream of impinging point for O/F of 1.0, 1.2, 1.6, 1.8, 2.1, and 2.5, respectively. The outer probability density contour was 5×10^{-4} mm^{-2} and the increment between contours was 3×10^{-3} mm^{-2}. The dark (blue) line enclosed the area of measured flame temperatures of impinging combustion of NTO/MMH above 1800 K.

IV. Conclusions

In this NTO/MMH impinging combustion experiment with 0.3/0.3 mm orifices and a $+30/-30$ deg impinging angle, the observations showed that the best mixing and combustion occurred at $O/F = 1.2$ with the longest flame length of ~80 mm. At higher O/F (>1.2), partially premixed diffusion-type flames were observed and the flame lengths were shorter due to poor mixing or incomplete combustion. The results also demonstrated an in-depth relation between the cold-flow impinging spray observations of NTO/MMH simulants and the observation of hot-fire impinging combustion of NTO/MMH. The analysis verified that the ignition of NTO/MMH impinging combustion was controlled by the local evaporation rate of MMH droplets in the downstream of the impinging point. Because of the fast evaporation of the droplets after ignition, the mixing characteristics or the mixture ratio profile after the ignition position was almost conserved. Thus, the predicted temperature distributions from cold-flow impinging experiments of NTO/MMH simulants at the corresponding ignition position can adequately described the shapes and locations of the high-temperature zone in hot-fire observations. However, because of the thermal expansion and the strong radiative heat loss, the flame distributed wider with lower temperatures in the hot-fire observations.

References

[1] Lecourt, R., and Foucaud, R., "Hypergolic Propellant Burning Spray Visualization by Laser Sheet Method: Application to Droplet Size and Liquid Concentration Measurements," *Experimental and Numerical Flow Visualization, 1993 ASME Winter Annual Meeting*, edited by B. Khalighi, Fed-Vol. 172, American Society of Mechanical Engineers, New York, 1993, pp. 173–181.

[2] Seamans, T. F., and Vanpee, M., "Development of a Fundamental Model of Hypergolic Ignition in Space-Ambient Engines," *AIAA Journal*, Vol. 5, No. 9, 1967, pp. 1616–1624. doi:10.2514/3.4259

[3] Rupe, J. H., "The Liquid Phase Mixing of A Pair of Impinging Streams," Jet Propulsion Laboratory, California Institute of Technology, Pasadena, CA, JPL Progress Rept. 20-195, 1953.

[4] Rupe, J. H., "A Correlation Between the Dynamic Properties of a Pair of Impinging Streams and the Uniformity of Mixture Ratio Distribution in the Resulting Spray," Jet Propulsion Laboratory, California Institute of Technology, Pasadena, CA, JPL Progress Rept. 20-209, 1956.

[5] Won, Y. D., Cho, T. H., and Yoon, W. S., "Effect of Momentum Ratio on

the Mixing Performance of Unlike Split Triplet Injectors," *Journal of Propulsion and Power*, Vol. 18, No. 4, 2002, pp. 847–854. doi:10.2514/2.6008

[6] Riebling, R. W., "Criteria for Optimum Propellant Mixing in Impinging-Jet Injector Elements," *Journal of Spacecraft and Rockets*, Vol. 4, No. 6, 1967, pp. 817–819. doi:10.2514/3.28966

[7] Ashgriz, N., Brocklehurst, W., and Tally, D., "Mixing Mechanism in a Pair of Impinging Jets," *Journal of Propulsion and Power*, Vol. 17, No. 3, 2001, pp. 736–749. doi:10.2514/2.5803

[8] Koh, H., Kim, D., and Yoon, Y., "Correction of Attenuation Effects in Dense Sprays Using Planar Imaging Technique," *Proceedings of the 10th International Symposium on Flow Visualization*, F0188, Optimage, Ltd.. Midlothian, England, U.K., Aug. 2002.

[9] Jung, K., Lim, B., Yoon, Y., and Koo, J.-Y., "Comparison of Mixing Characteristics of Unlike Triplet Injectors Using Optical Patternator," *Journal of Propulsion and Power*, Vol. 21, No. 3, May–June 2005, pp. 442–449. doi:10.2514/1.12884

[10] Sankar, S. V., Maher, K. E., Robart, D. M., and Bachalo, W. D., "Rapid Characterization of Fuel Atomizers Using an Optical Patternator," *Journal of Engineering for Gas Turbines and Power*, Vol. 121, July 1999, pp. 409–414. doi:10.1115/1.2818488

[11] Yuan, T., and Chen, C., "Observations of the Spray Phenomena of Unlike-doublet Impinging Jets," *Proceedings of the 11th International Symposium on Flow Visualization*, F064, Optimage, Ltd.. Midlothian, England, U.K., Aug. 2004.

[12] Yuan, T., Chen, C., and Huang, B., "Optical Observation of the Impingements of Nitrogen Tetroxide/Monomethylhydrazine Simulants," *AIAA Journal*, Vol. 44, No. 10, 2006, pp. 2259–2266. doi:10.2514/1.18375

[13] Schindler, R. C., and Schoenman, L., "Development of a Five-Pound Thrust Bipropellant Engine," *Journal of Spacecraft and Rockets*, Vol. 13, No. 7, July 1976, pp. 435–442. doi:10.2514/3.57105

[14] Stechman, R. C., and Smith, J. A., "Monomethyl Hydrazine vs. Hydrazine Fuels: Test Results Using Flight Qualified 100 lb_f and 5 lb_f Bipropellant Engine Configurations," AIAA Paper 83-1257, 1983.

[15] Shaddix, C. R., "Correcting Thermocouple Measurements for Radiation Loss: A Critical Review," American Society Of Mechanical Engineers International Paper HTD99-282, 1999.

[16] Wall, R. N., Basch, D. R., and Jacobson, D. L., "High-Temperature Spectral Emissivity of Several Refractory Elements and Alloys," *Journal of Materials Engineering and Performance*, Vol. 1, No. 5, 1992, pp. 679–684. doi:10.1007/BF02649249

[17] Lai, W. H., Huang, W., and Jiang, T. L., "Characteristic Study on the Like-Doublet Impinging Jets Atomization," *Atomization and Sprays*, Vol. 9, No. 3, May–June 1999, pp. 277–289.

[18] Vassallo, P., Ashgriz, N., and Boorady, F. A., "Effect of Flow Rate on the Spray Characteristics of Impinging Water Jets," *Journal of Propulsion and Power*, Vol. 8, No. 5, Sept.–Oct. 1992, pp. 980–986. doi:10.2514/3.23582

[19] McCarthy, M. J., and Molloy, N. A., "Review of Stability of Liquid Jets and the Influence of Nozzle Design," *Chemical Engineering Journal*, Vol. 7, 1974, pp. 1–20.

R. Lucht
Associate Editor